Study of the Electronic Structure for Te-Doped FeSe Superconductor Prepared by Solvothermal Method

H.-H. Zhao, X.-Y. Jia, J.-D. Shen,
Y.-J. Lai, L.-S. Feng and Q. Li*

School of Physics, Southeast University, Nanjing 211189, PR China

The samples of $FeSe_{1-x}Te_x$ ($x = 0$, 0.1, 0.2) were successfully prepared by solvothermal method. The results of X-ray diffraction show that the purity of the samples prepared by the solvothermal method is higher than that of the samples prepared by the solid-state reaction and flux method. The superconducting transition temperature (T_c) of $FeSe_{1-x}Te_x$ for $x = 0$, 0.1, 0.2 samples is near 9.3 K, 12.4 K, and 13.9 K, respectively, which is a bit higher than that of bulk samples. The electronic structures of these samples are investigated by X-ray photoemission spectroscopy and X-ray absorption spectroscopy. The Fe $2p$ X-ray photoemission spectroscopy spectra shift to higher binding energy by Te doping due to the increase in hole densities. X-ray photoemission spectroscopy spectra of Se $3d$ and Te $3d$ shift to higher binding energy and lower binding energy, respectively, resulting from the charge transfer between Se and Te. It is suggested that the hybridization between Fe $3d$ and Se $4p$ is strengthened. Our results imply that the hybridization between Fe $3d$ and Se $4p$ probably plays an important role in superconductivity.

topics: Te-doped FeSe, solvothermal method, X-ray photoemission spectroscopy (XPS)

1. Introduction

The effect of hybridization on superconductivity has been studied in literature by theoretical calculations [1–7]. For superconductors, the pairing mechanism plays an important role in the mechanism of superconductivity [8]. The valence electrons of atoms causing the emergence of superconductivity are divided into two parts. One part is involved in the formation of chemical bonds, and the other part is the formation of Cooper pairs [9, 10]. Spin fluctuation is one of the main factors in the formation of electron Cooper pairs. The doped electrons or holes in the superconductor destroy the long-range magnetic order, but there is still a strong correlation between the electrons or holes, which leads to strong spin fluctuations [11]. Spin–orbit coupling causes splitting and lifting of the degeneracy at the center of the Brillouin zone, and the zone center splitting reflects the hybridization of the d_{xz}, d_{yz} orbitals with the p orbitals of the neighboring chalcogenide atoms [12]. Due to the attractive interaction, the electrons near the Fermi surface form superconducting pairs, which changes the electron distribution near the Fermi surface. The change in the Fermi pocket is caused by the change in carrier concentration. In the case of element substitution or pressure, the strong hybridization between d and p leads to a decrease in the magnetic moment, which is favorable for the evolution of the superconductivity [13–15]. Therefore, the hybridization is reasonably considered to play an important role in the evolution of the superconductivity.

FeSe has the simplest crystal structure with $P4/nmm$ space group, and its superconducting transition temperature (T_c) is $\simeq 8$ K. The temperature T_c raises to $\simeq 15$ K at 50% Te substitution [16]. The introduction of effective carriers by element doping results in a change in the density of states around Fe sites, leading to a change in hybridization strength between Fe $3d$ and chalcogen p orbitals [17]. Therefore, it is necessary to elucidate the mechanism of superconductivity in the FeSe family.

High-quality samples are of great significance to researchers studying physical properties and superconducting mechanisms. The low-temperature chemical solution method has been proven to be feasible by relevant studies [18–21]. For FeSe, T_c can vary from 3.2 to 10 K by adjusting the reaction conditions. In the case of FeSe prepared by the solvothermal method, its transition temperature ($T_c \simeq 10$ K) is higher than that of FeSe prepared by the high-temperature method of ($\simeq 8$ K). It is still unclear whether T_c of Te-doped FeSe samples prepared by this method is higher than that of samples prepared by the high-temperature method.

The percentage of atoms from EDS in various points for $FeSe_{1-x}Te_x$ ($x = 0$, 0.1, 0.2) samples.

Samples	FeSe		$FeSe_{0.9}Te_{0.1}$			$FeSe_{0.8}Te_{0.2}$		
At [%]	Fe [%]	Se [%]	Fe [%]	Se [%]	Te [%]	Fe [%]	Se [%]	Te [%]
Point 1	49.9	50.1	50.3	45.1	4.6	49.4	42.9	7.7
Point 2	48.4	51.6	50.3	46.1	3.6	50.0	42.6	7.4
Point 3	49.3	50.7	49.8	45.5	4.7	49.6	32.8	7.6

Therefore, in this work, the samples of $FeSe_{1-x}Te_x$ ($x = 0$, 0.1, 0.2) are successfully prepared by the solvothermal method. The temperature T_c increases with increasing Te content, and T_c of the samples prepared by solvothermal method is a bit higher than that of the samples prepared by the solid-state reaction method. The electronic structures of samples are investigated by X-ray photoemission spectroscopy (XPS) and X-ray absorption spectroscopy (XAS). Our results imply that the change in ligand environment at the Fe site after Te doping in FeSe leads to the increase in the strengthening of the hybridization between Fe $3d$ and Se $4p$, thus leading to the enhancement of superconductivity of the Te-doped samples.

2. Experimental details

The samples of $FeSe_{1-x}Te_x$ ($x = 0$, 0.1, 0.2) were prepared by the solvothermal method using a low-temperature chemical solution. The raw chemicals include selenium powder (Se), tellurium powder (Te), iron (II) sulfate heptahydrate ($FeSO_4 \cdot 7H_2O$), sodium hydroxide (NaOH), polyvinylpyrrolidone (PVP), and ethylene glycol (EG). The preparation process can be divided into three major steps: preparation of selenium-containing solution, sintering process in reaction kettle and centrifugation process, and drying of the solutions [22]. The crystalline structures of the samples were measured by X-ray diffraction (XRD) with Cu K_α ray as sources. The scanning angle range was 10–80° with a step size of 0.02°. Scanning electron microscopy (SEM) and energy dispersive spectrometer (EDS) equipped with Inspect 50, FEI Company, were used for morphology analysis and composition analysis. The magnetic properties of the samples were measured in a Quantum Design Physical Property Measurement System (PPMS) in the temperature range of 5–20 K with a magnetic field of 10 Oe. X-ray absorption spectroscopy (XAS) measurements were performed in the total electron yield (TEY) mode at the photoelectron spectroscopy experimental station of Beijing Synchrotron Radiation Facility at the Institute of High Energy Physics, Chinese Academy of Sciences. X-ray photoemission spectroscopy (XPS) measurements were performed at the Analysis and Test Center of Southeast University with an Al target of 1486.6 eV. The XPS data were calibrated to the C $1s$ line at 284.6 eV.

3. Results and discussions

The XRD patterns of $FeSe_{1-x}Te_x$ ($x = 0$, 0.1, 0.2) samples are shown in Fig. 1. The curve labeled "FeSe-PDF" is taken from the database as "Powder Diffraction File" using MDI JADE software. The results are in good agreement with the JCPDS card 85-0735 with the space group $P4/nmm$. A weak peak of impurity phase at 45°C in $FeSe_{0.9}Te_{0.1}$ and $FeSe_{0.8}Te_{0.2}$ samples can be observed, which is due to the existence of $FeTe_2$. For other preparation methods, more impurities, such as Fe_3O_4 and Fe_7Se_8, were reported [23, 24]. Thus, the purity of the samples prepared by the solvothermal method is higher than that by other methods. The full width at half maximum (FWHM) of the diffraction peaks increases with increasing Te content, indicating a decrease in the grain size. With the increase in Te content, the XRD peaks shift to lower angles because the ion radius of Te (0.221 nm) is larger than that of Se (0.198 nm), suggesting that Te^{2-} ions are successfully incorporated into Se sites in FeSe by solvothermal method.
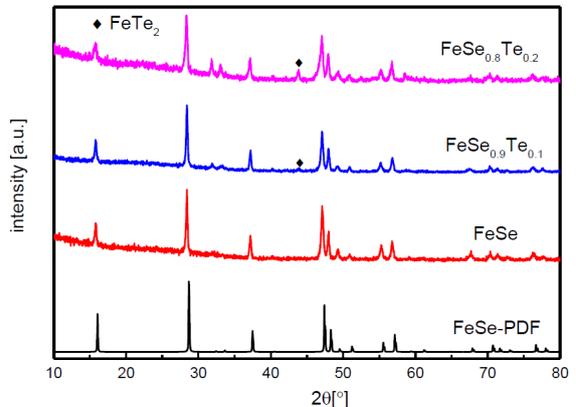
Fig. 1. The XRD patterns of $FeSe_{1-x}Te_x$ ($x = 0$, 0.1, 0.2) samples.
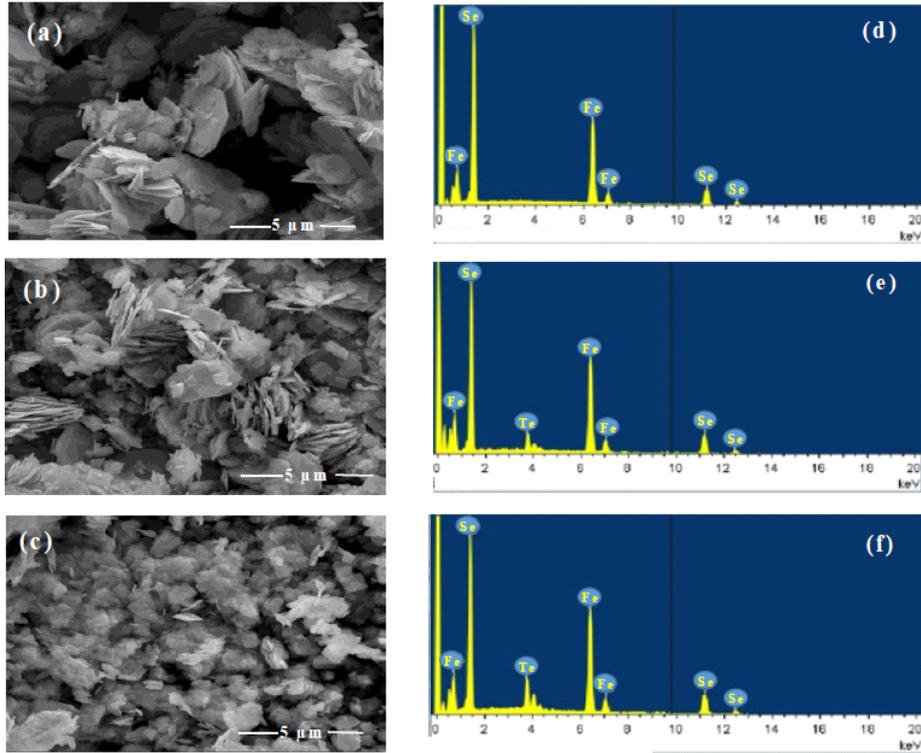
Fig. 2. (a)–(c) SEM micrograph of $FeSe_{1-x}Te_x$ ($x = 0$, 0.1, 0.2) samples; (d)–(f) EDS of $FeSe_{1-x}Te_x$ ($x = 0$, 0.1, 0.2) samples.

In order to further observe the micromorphology and determine the composition of constituent elements, SEM and EDS of $FeSe_{1-x}Te_x$ ($x = 0$, 0.1, 0.2) samples were measured, as shown in Fig. 2 and Table I. It can be seen that these samples show a two-dimensional (2D) quadrangle nano-flake morphology. The size of nano-flake ranges from hundreds of nanometers to more than 10 microns, and the thickness ranges from 10 to 150 nm. The two-dimensional characteristics of the samples prepared by the hydrothermal method are more obvious than of those prepared by the solid-state reaction method [25]. As for the atomic ratio of elements for Fe, Se, and Te in these samples, it can be seen in Table I that the actual contents of the samples are substantially the same as the nominal compositions.

The magnetic susceptibility measurements of $FeSe_{1-x}Te_x$ ($x = 0$, 0.1, 0.2) were performed, as shown in Fig. 3. The onset superconducting transition temperature of FeSe is 9.3 K, as shown in Fig. 3a. For $FeSe_{0.9}Te_{0.1}$ and $FeSe_{0.8}Te_{0.2}$, the onset superconducting transition temperatures are near 12.4 and 13.9 K, respectively, as shown in Fig. 3b and c. The transition temperature T_c of $FeSe_{1-x}Te_x$ for $x = 0$, 0.1, 0.2 samples prepared by the solid-state reaction was reported to be near 8.5, 10, and 12.5 K, respectively [26–28]. It is indicated that T_c of samples in this work is a bit higher than that of reported bulk samples prepared by the solid-

state reaction method. Moreover, T_c gradually increases with the increase in Te content. The increase in T_c is related to the structural distortion caused by the substitution of Te^{2-} ions with larger radii [29]. The isovalent substitution of Te for Se in FeSe causes an increase in the density of states at the Fermi level and the hole-type carrier densities [30]. In addition, the magnetization–temperature (M–T) curves of $FeSe_{0.9}Te_{0.1}$ and $FeSe_{0.8}Te_{0.2}$ bend upward in low-temperature region, showing the behavior of ferromagnetic background, possibly due to the presence of Fe^{3+} from the oxidation of Fe^{2+} in air, excess iron in the polycrystalline samples prepared by solvothermal method [31], or NaOH deliquescences in air in the preparation process [22].

In order to determine the valence states and electronic structures of $FeSe_{1-x}Te_x$ ($x = 0$, 0.1, 0.2) samples, XPS spectra measurements have been carried out, as shown in Figs. 4–7, and the indicated peak positions are shown in Table II. The wide scan XPS spectra of samples are shown in Fig. 4a. The peaks of each element including Fe $2p$, Se $3d$, and Te $3d$ have been shown. Other peaks, such as C $1s$ and O $1s$, have been also present. The XPS spectra of Fe $2p$ are shown in Fig. 4b.

The fitted Fe $2p$ spectra of $FeSe_{1-x}Te_x$ ($x = 0$, 0.1, 0.2) are depicted in Fig. 5a–c. The peaks of Fe $2p_{3/2}$ and $2p_{1/2}$ at ~ 711.0 eV and 725.0 eV are due to spin orbital splitting corresponding to Fe^{3+}. The peaks at 709.0 eV and 722.0 eV correspond
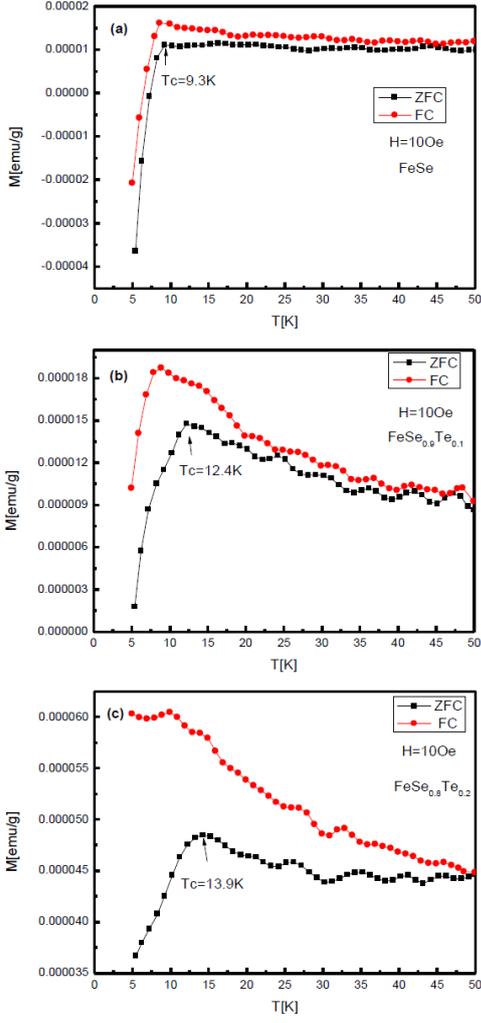
Fig. 3. The M–T diagrams of (a) FeSe, (b) FeSe$_{0.9}$Te$_{0.1}$, and (c) FeSe$_{0.8}$Te$_{0.2}$ samples.

Fig. 4. XPS spectra of (a) wide-scan and (b) Fe $2p$ spectra of FeSe$_{1-x}$Te$_x$ ($x = 0$, 0.1, 0.2) samples.
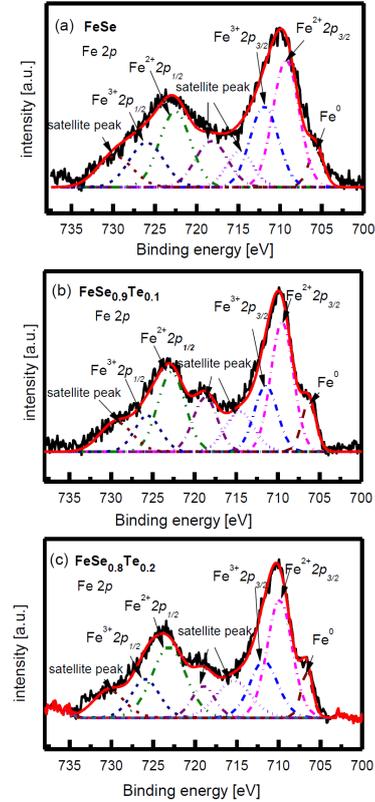
Fig. 5. (a)–(c) The fitted Fe $2p$ spectra of FeSe, FeSe$_{0.9}$Te$_{0.1}$, and FeSe$_{0.8}$Te$_{0.2}$, respectively. The black curves correspond to the raw data. The red and dashed curves correspond to the fitted data.

to Fe^{2+} [32, 33]. The small peak at 706.0 eV corresponds to Fe^0, which is due to the presence of excess Fe probably at the interstitial site in these samples [34]. The intensity of the peak at 706.0 eV increases after Te doping, which indicates that Te doping changes the ligand environment around Fe, leading to an increase in the content of interstitial iron [35]. The peak of Fe^{2+} $2p$ shifts to higher binding energy with the increase in Te content in FeSe, resulting from an increase in hole density. The balance between electrons and hole carriers (caused by the generation of superconductivity) is tuned by the expansion of the c-axis of the unit cell, leading to an increase in the hole density and a decrease in the electron density [36].

The XPS spectra of Se $3d$ and Te $3d$ for FeSe$_{1-x}$Te$_x$ ($x = 0$, 0.1, 0.2) are measured, as shown in Figs. 6 and 7. Two peaks of Se $3d$ at 53.0 eV and 54.0 eV corresponding to Se $3d_{5/2}$ and $3d_{3/2}$ are shown in Fig. 6b and Fig. 6c, which is consistent with another reference [37]. In addition,

Fig. 6. (a) Se $3d$ spectra of FeSe$_{1-x}$Te$_x$ ($x =$0, 0.1, 0.2) samples; (b)–(d) the fitted Se $3d$ spectra for FeSe, FeSe$_{0.9}$Te$_{0.1}$, and FeSe$_{0.8}$Te$_{0.2}$, respectively. The black curves correspond to the raw data. The red curves and the dashed curves correspond to the fitted data.

a small peak at 56.0 eV is known to originate from Se^{4+} in SeO$_2$ [38]. It is indicated that the valence state of selenium is mainly negative divalent in these samples. The peak positions of Se $3d$ shift to higher binding energy after Te doping in FeSe.

For Te $3d$ spectra of FeSe$_{0.9}$Te$_{0.1}$ and FeSe$_{0.8}$Te$_{0.2}$ samples, in order to observe the change clearly, the Te $3d_{5/2}$ spectra are shown in Fig. 7 in which two peaks at 572.3 eV and 575.4 eV correspond to Te^{2-} and Te^{4+}, respectively. A small amount of Te^{4+} originates from TeO$_2$ impurities on the surface [39]. The positions of Se $3d$ and Te $3d$ shift to higher binding energy and lower binding energy, respectively, which is associated with the change in valence state. The change in the number of holes is associated with the change in valence state, which leads to the change in binding energy for XPS spectra of Se $3d$ and Te $3d$. Through the study of Se K edge and Te K edge XAS spectra, it was suggested that the number of Se $4p$ holes increased after Te doped in FeSe, that the hybridization between Fe $3d$ and Se $4p$ was enhanced, and also that the number of Te $5p$ holes decreased, which was due to the charge transfer between Se and Te [29]. Thus, it is suggested that the hybridization between Fe $3d$ and Se $4p$ is strengthened after Te doping.

Figure 8 shows the XAS spectra of Fe L edge of FeSe$_{1-x}$Te$_x$ ($x = 0$, 0.1, 0.2). Two main absorption peaks of L_3 ($2p_{3/2}$) at 708.8 eV and L_2 ($2p_{1/2}$) at 722.1 eV are observed in Fig. 8a due to the spin–orbit splitting. The absorption peaks
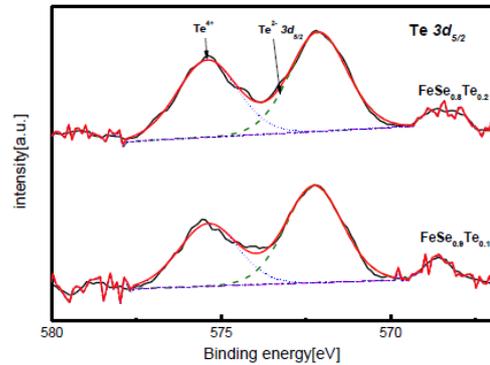
Fig. 7. (a) The fitted Te $3d_{5/2}$ spectra for FeSe$_{0.9}$Te$_{0.1}$ and FeSe$_{0.8}$Te$_{0.2}$. The black curves correspond to the raw data. The red and dashed curves correspond to the fitted data.

are attributed to the dipole transition from $2p$ to $3d$ ($2p^63d^6$–$2p^53d^7$). The shoulder at higher photon energy is associated with the covalent nature of Fe and Se conduction electrons [40–43]. The Gaussian fitting of Fe L edge spectra was performed as shown in Fig. 8b–d. The peak A around 707.1 eV is attributed to Fe^0. The peak B around 708.8 eV originates from Fe^{2+}. The peak C around 710.0 eV relates to the interaction of Fe and Se. The intensity of peak C

251

TABLE II

The peak positions of Fe $2p$, Se $3d$, and Te $3d$ XPS spectra for $FeSe_{1-x}Te_x$ ($x = 0$, 0.1, 0.2).

Samples		FeSe	$FeSe_{0.9}Te_{0.1}$	$FeSe_{0.8}Te_{0.2}$
Fe $2p$	Fe^0	705.7	706.3	706.7
	Fe^{2+} $2p_{3/2}$	709.3	709.5	709.9
	Fe^{3+} $2p_{3/2}$	711.9	711.4	711.8
	Fe^{2+} satellite peak	714.8	714.4	715.4
	Fe^{3+} satellite peak	718.2	718.7	719.0
	Fe^{2+} $2p_{1/2}$	722.6	722.8	723.2
	Fe^{3+} $2p_{1/2}$	726.0	725.6	725.9
	Fe^{3+} satellite peak	729.8	729.4	730.3
Se $3d$	Se^{2-} $3d_{5/2}$	52.7	53.4	53.5
	Se^{2-} $3d_{3/2}$	54.1	54.8	54.9
	Se^{4+}	56.6	57.6	56.6
Te $3d_{5/2}$	Te^{2-} $3d_{5/2}$	–	572.3	572.1
	Te^{4+}	–	575.4	575.4
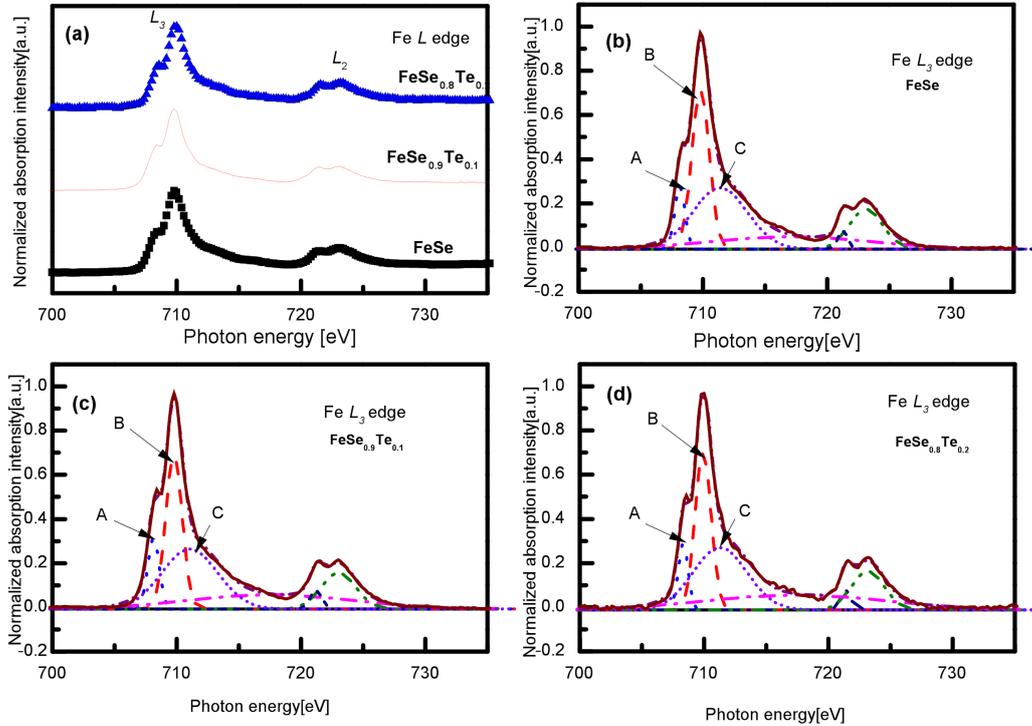
Fig. 8. (a) Normalized Fe L edge x-ray absorption spectra for $FeSe_{1-x}Te_x$ ($x = 0$, 0.1, 0.2); (b, c) the Gaussian fitted spectra for $FeSe_{1-x}Te_x$ ($x = 0$, 0.1, 0.2).

decreases with increasing Te content, resulting in an enhancement of the hybridization of Fe and Se. The valence band spectra demonstrate the hybridization between Fe $3d$ and Se $4p$ orbitals in Te-doped samples [44, 45]. The peak at around 4 eV, representing the hybridization between Fe $3d$ and Se $4p$, shows a broadening and shifts to lower binding energy with increasing Te content, indicating the stronger hybridization between Fe $3d$ and Se $4p$. For Te-doped FeSe samples, the density of carriers increases, leading to the enhancement of the inter-band

hybridization. Therefore, the hybridization plays an important role in the evolution of superconductivity.

4. Conclusions

In this paper, $FeSe_{1-x}Te_x$ ($x = 0$, 0.1, 0.2) samples were successfully prepared by a low-temperature solvothermal method using nontoxic and soluble iron, selenium, and tellurium sources as

starting materials. The purity of the samples was higher than that of the samples prepared by the conventional method. The diffraction peaks shifted to lower angles due to Te doping. The samples exhibit uniform layered two-dimensional nano-flakes. The superconducting transition temperature (T_c) of $FeSe_{1-x}Te_x$ for $x = 0$, 0.1, 0.2 is near 9.3 K, 12.4 K, and 13.9 K, respectively. The superconducting transition temperature of samples prepared by the solvothermal method is a bit higher than that of samples prepared by solid-state reaction. For Te-doped samples, T_c is improved due to the structure distortion. Meanwhile, the M–T curves are bent upward in the low-temperature region because the samples contain a small amount of Fe^{3+} and residual iron. The Fe $2p$ XPS spectra indicate that the iron element has a small amount of trivalent, and the content of interstitial iron increases due to the change of ligand environment at around Fe sites after Te doping in FeSe. The Fe $2p$ XPS spectra shift to higher binding energy after Te doping in FeSe due to the decrease in electron densities and the increase in hole densities. The Se $3d$ and Te $3d$ XPS spectra shift to higher binding energy and lower binding energy, respectively, which is due to the charge transfer between Se and Te. The Fe L edge spectra suggest the enhancement of hybridization between Fe and Se with the increasing Te content in FeSe. These results indicate that the hybridization between Fe $3d$ and Se $4p$ plays an important role in superconductivity.

Acknowledgments

References

[1] E.S. Caixeiro, A. Troper, *Phys. Rev. B* **82**, 014502 (2010).

[2] G.M. Japiassú, M.A. Continentino, A. Troper, *Phys. Rev. B.* **45**, 2986 (1992).

[3] E.S. Caixeiro, A. Troper, *Physica C.* **460**, 712 (2007).

[4] H. Suhl, B.T. Matthias, L.R. Walker, *Phys. Rev. Lett.* **3**, 552 (1959).

[5] J. Kondo, *Prog. Theor. Physics.* **29**, 1 (1963).

[6] J. Zieliński, P. Zawadzki, *Z. Phys. B, Condens. Matter.* **72**, 261 (1988).

[7] W. Wiethege, P. Entel, B. Mühlschlegel, *Z. Phys. B, Condens. Matter.* **47**, 35 (1982).

[8] Y. Bang, G.R. Stewart, *J. Phys. Condes. Matter.* **29**, 123003 (2017).

[9] C.H. Rüscher, M. Götte, *Solid State Commun.* **85**, 393 (1993).

[10] G. Blumberg, M.S. Kang, M.V. Klein, K. Kadowaki, C. Kendziora, *Science.* **278**, 1427 (1997).

[11] X. Chen, P. Dai, D. Feng, T. Xiang, F.-C. Zhang, *Natl. Sci. Rev.* **1** 371 (2014).

[12] P.D. Johnson, H.-B. Yang, J.D. Rameau, G.D. Gu, Z.-H. Pan, T. Valla, M. Weinert, A.V. Fedorov, *Phys. Rev. Lett.* **114**, 167001 (2015).

[13] V. Vildosola, L. Pourovskii, R. Arita, S. Biermann, A. Georges, *Phys. Rev. B.* **78**, 064518 (2008).

[14] S. Tsuda, N. Kikugawa, K. Sugii, S. Uji, S. Ueda, M. Arai, M. Nakajima, A. Iyo, H. Eisaki, *J. Phys. Soc. Jpn.* **86**, 053702 (2017).

[15] C. Ma, H. Yang, H. Tian, H. Shi, Z. Wang, J. Li, *J. Phys. Condens. Matter.* **25**, 115503 (2013).

[16] K.-W. Yeh, T.-W. Huang, Y.-L. Huang et al., *EPL* **84**, 37002 (2008).

[17] P.P. Singh, *J. Phys.-Condes. Matter.* **22**, 13550 (2010).

[18] U. Pachmayr, N. Fehn, D. Johrendt, *Chem. Commun.* **52**, 194 (2015).

[19] L. Chen, H. Zhan, X. Yang, Z. Sun, J. Zhang, D. Xu, C. Liang, M. Wu, J. Fang, *CrystEngComm.* **12**, 4386 (2010).

[20] L. Chen, X. Yang, X. Fu, C. Wang, C. Liang, M. Wu, *Eur. J. Inorg. Chem.* **2011**, 2098 (2011).

[21] M.-L. Li, Q.-Z. Yao, G.-T. Zhou, S.-Q. Fu, *CrystEngComm.* **12**, 3138 (2010).

[22] D. Li, D. Pan, W. Liu et al., *Chem. Mater.* **29**, 842 (2017).

[23] K.J.S. Silva, D.A. Landinez Tellez, C.A. Parra Vargas, D. Martinez Buitrago, C.A.C. Passos, I.M. Capucho, J.N.O. Pinto, V.T. Abílio, J. Albino Aguiar, *J. Supercond. Nov. Magn.* **30**, 1699 (2017).

[24] C. Dong, H. Wang, Z. Li, J. Chen, H.Q. Yuan, M. Fang, *Phys. Rev. B.* **84**, 224506 (2011).

[25] K. Onar, M.E. Yakinci, *J. Alloy. Compds.* **620**, 210 (2015).

[26] M.K. Wu, F.C. Hsu, K.W. Yeh et al., *Physica C.* **469**, 340 (2009).

[27] K. Park, J.W. Taylor, D. Louca, *J. Supercond. Nov. Magn.* **27**, 1927 (2014).

[28] R.W. Gómez, V. Marquina, J.L. Pérez-Mazariego, R. Escamilla, R. Escudero, M. Quintana, J.J. Hernández-Gómez, R. Ridaura, M.L. Marquina, *J. Supercond. Nov. Magn.* **23**, 551 (2010).

[29] C.L. Chen, C.L. Dong, J.L. Chen et al., *Phys. Chem. Chem. Phys.* **13**, 15666 (2011).

[30] H.H. Chang, J.Y. Luo, C.T. Wu, F.C. Hsu, T.K. Chen, P.M. Wu, M.K. Wu, M.J. Wang, *Physica C* **470**, S480 (2010).

[31] R. Viennois, E. Giannini, D. van der Marel, R. Černý, *J. Solid State Chem.* **183**, 769 (2010).

[32] P.S. Miedema, F.M.F. de Groot, *J. Electron. Spectrosc. Relat. Phenom.* **187**, 32 (2013).

[33] A.P. Grosvenor, B.A. Kobe, M.C. Biesinger, N.S. McIntyre, *Surf. Interface Anal.* **36**, 1564 (2004).

[34] T.S. Su, Y.W. Yin, M.L. Teng, Z.Z. Gong, M.J. Zhang, X.G. Li, *J. Appl. Phys.* **114**, 183901 (2013).

[35] H.H. Chang, J.Y. Luo, C.T. Wu et al., *Supercond. Sci. Technol* **24**, 105011 (2011).

[36] I. Tsukada, F. Nabeshima, A. Ichinose, S. Komiya, M. Hanawa, Y. Imai, A. Maeda, *Jpn. J. Appl. Phys.* **54**, 043102 (2015).

[37] T.-K. Chen, J.-Y. Luo, C.-T. Ke et al., *Thin Solid Films.* **519**, 1540 (2010).

[38] R. Würz, M. Rusu, T. Schedel-Niedrig, M.Ch. Lux-Steiner, H. Bluhm, M. Hävecker, E. Kleimenov, A. Knop-Gericke, R. Schlögl, *Surf. Sci.* **580**, 80 (2005).

[39] O.A. Balitskii, W. Jaegermann, *Mater. Chem. Phys.* **97**, 98 (2006).

[40] M.Y. Hacisalihoglu, E. Paris, B. Joseph, E. Yanmaz, N.L. Saini, *Phys. Chem. Chem. Phys.* **17**, 18131 (2015).

[41] A.C. Scheinost, R. Kirsch, D. Banerjee, A. Fernandez-Martinez, H. Zaenker, H. Funke, L. Charlet, *J. Contam. Hydrol.* **102**, 228 (2008).

[42] W.L. Yang, A.P. Sorini, C.-C. Chen et al., *Phys. Rev. B* **80**, 014508 (2009).

[43] N. D., P.A. Alvi, K.B. Garg, S. Dalela, *J. Supercond. Nov. Magn.* **27**, 1431 (2014).

[44] P. Mishra, H. Lohani, R.A. Zargar, V.P.S. Awana, B.R. Sekhar, *J. Phys. Condens. Matter.* **26**, 425501 (2014).

[45] T. Yokoya, R. Yoshida, Y. Utsumi et al., *Sci. Technol. Adv. Mater.* **13**, 054403 (2012).